Mechanisms of ion beam mixing in metals and semiconductors

K. Nordlund, M. Ghaly, and R. S. Averback

Additional information on J. Appl. Phys.

Mechanisms of ion beam mixing in metals and semiconductors

K. Nordlund,[a] M. Ghaly, and R. S. Averback

Materials Research Laboratory, University of Illinois, Urbana, Illinois 61801

Ion beam mixing was investigated in crystalline and amorphous semiconductors and metals using molecular dynamics simulations. The magnitude of mixing in an amorphous element compared to its crystalline counterpart was found to be larger by a factor of 2 or more. Mixing in semiconductors was found to be significantly larger than in a face-centered-cubic (fcc) metal of corresponding mass and atomic density. The difference in mixing between amorphous and crystalline materials is attributed to local relaxation mechanisms occurring during the cooling down phase of the cascade. Comparison of mixing in semiconductors and metals shows that short range structural order also has a significant influence on mixing. The mixing results in fcc metals indicate that the role of the electron–phonon coupling in the evolution of collision cascades may be less significant than previously thought. © *1998 American Institute of Physics.* [S0021-8979(98)02903-X]

I. INTRODUCTION

The mechanisms of damage production in solids during ion irradiation is of great practical interest for such fields as ion beam processing of materials, surface characterization, and reactor technology. Unfortunately the experimental possibilities for studying the processes occurring inside materials during irradiation are quite limited. Ion beam mixing, i.e., the local rearrangement of atoms due to irradiation,[1] is one of the few measurable quantities that is a direct consequence of collision cascade processes. Studies of the mechanisms of ion beam mixing using computational methods are therefore particularly interesting since the results can be compared with experiments. This makes possible both an elucidation of damage formation mechanisms in solids on an atomistic level and a test of the quantitative accuracy of the simulation models.

Ion beam mixing, or simply ''mixing,'' has been measured in many solids representing all classes of materials. A surprising result is that the amount of mixing per unit dose (measured in deposited damage energy per unit volume) is larger in Si than in most metals and ceramics in the same mass range.[1] In fact, mixing in several semiconductors, such as Ge, GaAs, and InP, seems anomalously large. These observations hold even for very low-temperature irradiations, in some cases less than 30 K, and they are independent of the type of irradiation particle,[1,2] indicating that neither radiation enhanced diffusion nor electronic excitation are likely explanations for these results.

There are two major differences between metals and semiconductors relevant for irradiation processes: semiconductors become amorphous upon irradiation, whereas metals do not, and the atomic packing density is higher in most metals than in semiconductors. There has been some indications that mixing in amorphous structures is larger than in the crystalline ones.[2] This is expected within thermal spike models of mixing, since the thermal conductivities of amorphous materials are much less than those of their crystalline counterparts.

Most previous theoretical studies of mixing have been based on analytical models or binary collision approximation computer simulations.[3–7] While these models have elucidated many aspects of mixing, they do not provide a truly atomistic picture of the mechanisms of mixing. Molecular dynamic (MD) computer simulations, on the other hand, are ideally suited for studying mixing as they include all the atomic collision processes involved. Although a few studies have reported mixing values in Si at very low energies,[8] no previous MD study has focused on elucidating the specific roles of ballistic and heat spike processes for mixing in semiconductors, or have compared mixing systematically either between different kinds of materials or between simulation and experiment.

In the present article, we use MD computer simulations to examine the mechanisms of mixing in different materials. The aim is to clarify how different materials properties, such as the atomic number, density, melting temperature, and structure influence mixing. We treat a wide variety of materials, namely crystalline Si, Ge, Al, Ni, Cu, Pt, and Au, and amorphous Si, Ge, Al, and Au. Our first results for silicon and crystalline Al have been presented in a previous letter.[9] The present study extends this previous work, and also treats heavier elements and amorphous metals to further elucidate the mixing mechanisms.

II. CALCULATION PRINCIPLES

We used classical MD methods to simulate full collision cascades. A linkcell calculation[10] and variable time step[11] were employed to speed up the simulations. The atoms were arranged in cubic simulation cells, which contained between 20 and 40 atoms for every electron volt of kinetic energy assigned to the initial recoil. In the 10 keV simulations, we used cells with about 340 000 atoms for Al, 315 000 atoms for Si, and 260 000 atoms for the heavier elements. Periodic boundary conditions were applied on the cell, and the temperature of the atoms in the outermost atom layers was softly

a)Permanent address: Accelerator Laboratory, P.O. Box 43, FIN-00014 University of Helsinki, Finland; electronic mail: kai.nordlund@helsinki.fi

scaled towards 0 K to provide temperature control and ensure that the pressure waves emanating from cascades were damped at the borders. The cell sizes were initially equilibrated to zero pressure using a pressure control algorithm,[12] independently for the three spatial dimensions. During the cascade calculations the cell size was held fixed, since the usual pressure control algorithms are not suited for treating the strong pressures present in the center of the cascade.

To obtain a comprehensive picture of mixing, we simulated a variety of different amorphous and crystalline semiconductors and metals. Because of their interest in semiconductor manufacturing and the availability of good interatomic potentials, we chose silicon and aluminum to represent light elements. Al is very similar in mass and atomic density to Si, but quite different in the bonding structure, so comparison of Al and Si cascades can be instructive in elucidating the effect of the crystal structure and bonding type on cascade dynamics. We studied mixing in the energy range 400 eV–10 keV in both amorphous and crystalline Si and Al to obtain a comprehensive view of the mixing mechanisms in these elements. Similar comparisons were made between Cu, Ni, and Ge, between crystalline and amorphous Au, and crystalline Au and Pt.

The forces acting between atoms in silicon and germanium were calculated from the Stillinger–Weber three-body interatomic potential.[13] Since the potential is constructed to reproduce properties of solid, amorphous, and liquid Si, it is particularly well suited for the present study.[13,14] The Ge potential was modified to reproduce the melting point correctly.[15] To realistically treat strong collisions a repulsive potential derived from *ab initio* calculations[16] was smoothly joined to the three-body potential at short interaction distances.[17] We have recently shown that ion beam mixing in Si is not sensitive to the choice of the interatomic potential,[15] so our choice of potential should not affect the results presented here.

Embedded atom method (EAM) potentials were used to describe the atomic interactions in the metals,[18,19] with the Ziegler–Biersack–Littmark universal interatomic potential[20] fitted to the EAM potential at short interactions. The fit of the repulsive potential was fine-tuned so that the fitted potential gave a realistic value of the threshold displacement energy.

The amorphous Si structure was created by first equilibrating liquid Si at 3000 K for 10 ps, then quenching it to 0 K at a rate of 0.02 K/fs for 150 ps. This quench produced an amorphous Si structure with an average potential energy of -4.11 eV/atom at 0 K (to be compared with the crystalline Si potential energy of -4.33 eV). For Ge, we similarly obtained -3.00 eV, to be compared with -3.17 eV for the ground state of our modified potential. Additional annealing steps of the cell did not lower the potential energy further, which indicates that these Si and Ge structures are the lowest-energy amorphous phases of the Stillinger–Weber potentials employed.

For creating amorphous Al and Au, initial heat spikes at 2000 K and a number of subsequent heating and slow quenching steps were used to obtain an amorphous structure. Contrary to the results in silicon, we did not find any unique amorphous phase in these metals. The annealing steps continued to increase the amount of order in the cell, and decrease the potential energy toward the equilibrium value. As an aside, we note that such behavior is predicted by Granato's interstitialcy theory of amorphous solids and liquids.[21] We chose amorphous structures obtained after several successive annealing simulations in which the initial heating temperature was lowered for every step. Thus, we obtained structures which were relatively stable towards heating to moderate temperatures of the order of 300 K. For Al the amorphous structure had a potential energy of -3.28 eV (crystalline Al at 0 K has -3.36 eV) and for Au -3.89 eV (c-Au has -3.93 eV). Both structures had appreciable short range order resembling the close-packed face-centered-cubic (fcc) structure, but no long-range order.

We emphasize that because a unique amorphous phase was not identified for the metals within the EAM formalism, and because very little is known about the nature of real amorphous metals, our mixing results in a-Al and a-Au are meaningful primarily in providing a contrasting point of view to the results in the crystalline phase.

The collision cascades were initiated by giving one atom in the cell a recoil energy of 400 eV, 2 keV, or 10 keV. The initial recoil direction was chosen randomly, and the initial recoil position subsequently so that the primary recoil and energetic secondary recoils remained inside the cell borders throughout the simulation. Electronic stopping powers[22,23] were included in the simulations as a nonlocal frictional force affecting all atoms with a kinetic energy higher than 10 eV.

The electron–phonon coupling was not included in the present simulations. Koponen[4] has derived an analytical model which suggests that the low values of mixing observed in Ni, Pd, and Pt may be a consequence of the short relaxation time in the coupling of the electronic and atomic subsystems. On the other hand, these same metals with a strong electron–phonon coupling also have high melting points and elastic moduli. The high melting points and strength of the material could also result in low mixing values. By excluding the electron–phonon coupling in Pt and Ni, we test whether a purely conservative heat spike model can explain the experimental mixing results.

To obtain the time dependence of mixing, the positions of all atoms were output at 10–15 instants during an event and the squares of the atomic displacements $[r_i(t) - r_i(t=0)]^2$ were summed over all atoms in the simulation cell. We verified that no displacement of the cell center of mass and no cell rotation occurred since they would have affected the value of $[r_i(t) - r_i(t=0)]$. The mixing parameter Q was determined using the expression

$$Q = \frac{\Sigma_i [r_i(t) - r_i(t=0)]^2}{6n_0 E_{D_n}}, \tag{1}$$

where n_0 is the atomic density and E_{D_n} the deposited nuclear energy. E_{D_n} was obtained from the difference of the initial recoil energy and the total energy lost to electronic stopping.

TABLE I. Average total (Q) and short-range (Q') mixing and the number of displaced atoms N_{displ} in cascades in Si and Al. The error bars are estimates of the deviation from the average between different cascades. Q is the total mixing and Q' a measure of the thermal spike mixing, from which long-range channeled particles have been discounted.

El.	Cascade E (keV)	E_{D_n} (keV)	Q (Å^5/eV)	Q' (Å^5/eV)	N_{displ}
c-Si	0.4	0.35	6±11	3.0±1	27±2
	2.0	1.6	16±2	3.5±0.5	120±4
	10.0	7.5	15±3	3.5±0.5	550±40
a-Si	0.4	0.35	15±2	8±1	66±9
	2.0	1.6	21±1	12±1	420±30
	10.0	7.5	30±1	17±1	2500±200
c-Al	0.4	0.36	4.1±0.2	3.3±0.2	80±5
	2	1.7	9±1	4±1	230±20
	10	7.9	9±1	4±1	800±100
a-Al	0.4	0.35	25±1	21±1	200±20
	2.0	1.6	28±1	20±1	1200±40
	10	7.4	41±5	28±4	8000±1000
c-Ge	10.0	7.6	30±3	20±2	2300±100
a-Ge	10.0	7.6	70±5	57±5	9800±400
c-Ni	10.0	7.8	4.3±0.2	3.4±0.2	1400±40
c-Cu	10.0	7.9	13±1	12±1	3000±50
c-Pt	10.0	7.3	22±1	17±1	2330±20
c-Pt	25.0	17.7	45±3	25±2	6800±200
c-Au	10.0	7.0	58±2	33±2	3350±50
a-Au	10.0	7.1	180±10	89±2	12 400±300

III. RESULTS AND DISCUSSION

The mixing results are summarized in Table I. These data in Table I represent averages of typically 5–7 cascade events for each initial recoil energy and material. The uncertainties given are the errors in the averages. Table I contains both the total mixing, Q, as defined in Eq. (1), and the mixing Q' which represents the contribution from atoms that have moved less than 10 Å from their initial locations. The latter quantity disregards the movement of energetic recoils. The choice of 10 E for the cut-off was motivated by plotting the integrated relative mixing

$$Q_I(r) = \frac{\int_0^r dQ(r)}{Q} \qquad (2)$$

as a function of the atom displacement distance for all atoms in the cell (see Fig. 1). The leveling-off of the mixing between 5 and 10 Å makes Q' reasonably insensitive to the cut-off distance in this region.[24] Also included in Table I are values for the number of atoms displaced more than half of a nearest-neighbor distance from their initial lattice site, N_{displ}.

A. Silicon and aluminum

The silicon results are presented in Table I and Figs. 1–4. Table I shows that mixing is substantially larger in a- than in c-Si. The added mixing, moreover, derives almost entirely from the difference in the short range mixing Q' (see Fig. 1). The long range mixing, $Q-Q'$, is the same for the crystalline and amorphous targets to within the uncertainties.

The difference in the mixing behavior can also be seen in Fig. 2, where the number of atoms that have been dis-
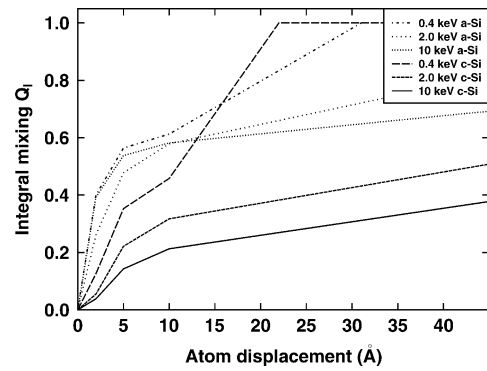

FIG. 1. Relative integrated mixing Q_I [see Eq. (2)] as a function of the displacement distance for Si cascades of different energies. The mixing is normalized so that the mixing at the maximum atom displacement is 1.0. The curves are averages over 2–4 cascade events.

placed from their initial locations a distance between r and $r+dr$ is plotted as a function of r. The greater number of atoms displaced short distances in the amorphous target is readily apparent, whereas beyond about 10 Å only minor differences are found between a- and c-Si. The final positions of all atoms displaced more than 0.2 Å after a 2 keV cascade are shown in Fig. 3 for c- and a-Si. It is immediately apparent that the number of displaced atoms is much larger in the amorphous material. It is also interesting to note that a few atoms have been displaced far from the core of the cascade in a-Si. These displacements, which are too small to be significant to the total mixing, are a consequence of the heat and pressure wave emanating from the cascade. Similar displacements are not present in c-Si since the crystal structure prevents such small displacements.

The number density of displaced atoms (Fig. 2) for $r > 5$ Å varies nearly as the inverse square of distance, which is indicative of collisional mixing. Moreover, since the long range mixing is nearly identical for crystalline and amorphous targets, channeling effects at these low energies must be insignificant. The larger short range mixing in a-Si might, at first glance, suggest that thermal spikes have greater influence in amorphous targets. A plot of the time dependence of mixing indicates otherwise, however. Figure 4 shows that at 0.3 ps most of the mixing is complete and the magnitudes of
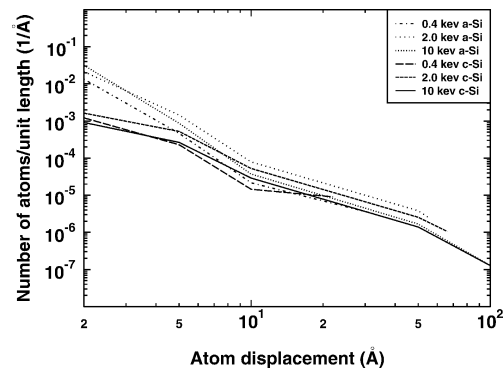

FIG. 2. Fraction of atoms that have been displaced a certain distance in cascade events in amorphous (a-) and crystalline (c-) Si.
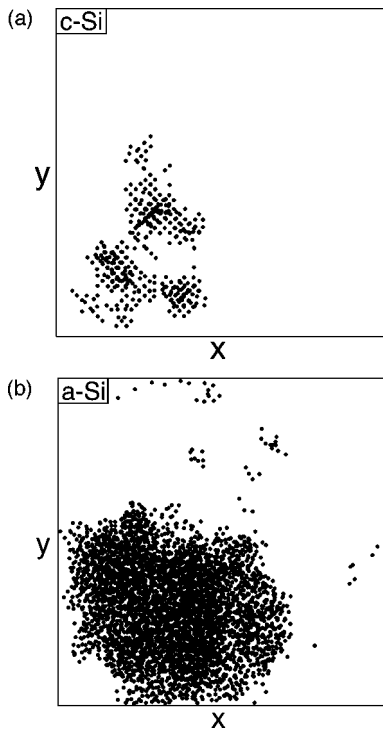
FIG. 3. Atoms displaced more than 0.2 Å in 2 keV cascades in crystalline and amorphous silicon. The atom positions are projected onto the xy plane. The cell size is 46 Å in both the x and y directions. Note that periodic boundary conditions were used in the simulations.

the mixing in the two structures are very similar at each of the recoil energies examined.

Following this initial displacement process, however, mixing in the amorphous phase creeps upward over the next few ps, while in the crystalline phase it creeps downward. The difference in mixing, therefore, derives from an atomic relaxation process that follows the collisional phase of the cascade. For the crystalline matrix, many atoms displaced short distances from their lattice sites return to them during the relaxation. For the amorphous phase, memory of the original site locations is lost as the local atomic configurations are rearranged, and so excited atoms randomly fall back
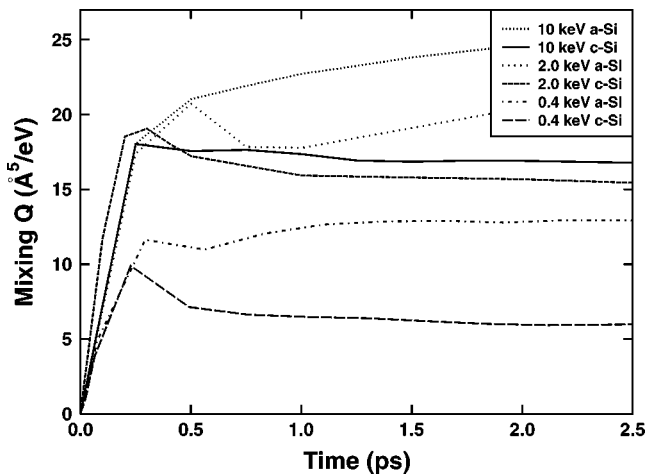

FIG. 4. Mixing as a function of time for individual representative cascade events in amorphous and crystalline Si.

to sites representing local minima in the potential energy. Thus, the atomic motion during the relaxation process adds to the mixing in a-Si but diminishes it in c-Si.

Whether the mixing in the later stages of the cascade in Si should be referred to as thermal spike mixing is arguable. While no extended spike is seen, it is likely that the local relaxation process is stimulated by the thermal agitation of the lattice in the vicinity of the cascade. Since hot liquidlike zones exists for about 1–2 ps in Si after the initiation of the cascade (cf. Fig. 6), it is clear that some regions of the cell will be close to the melting temperature for a few picoseconds. It is noteworthy that the amount mixing, or demixing, during this relaxation period is a significant fraction of that for collisional mixing. It occurs, moreover, while the atomic energies are a few tenths of eV. This suggests that in systems where chemical forces are involved, the movement of atoms during relaxation might be biased toward more or less mixing depending upon the direction of these forces.

Since Al has nearly the same atomic number and atomic density as Si, but different bonding and cohesive properties, a comparison of mixing in Si and Al further elucidates the bonding effect on mixing. The results in Table I show that the mixing parameter is smaller in c-Al than in either a- or c-Si, even though the number of displaced atoms N_{displ} is substantially larger in c-Al than in c-Si. The smaller mixing in Al, therefore, derives predominantly from the difference in long range mixing. The more close-packed structure and lower melting temperature of Al cause the heat spikes in Al to be somewhat more pronounced than in Si,[15] explaining why the number of displaced atoms is larger. Despite this larger number of atoms in the liquid zone of a cascade, which exists for only a few ps in Al, these atoms can move only very short distances, and thus, contribute less to the mixing than Si atoms that are displaced by longer range ballistic events.

The small, long-range ballistic mixing in Al may at first seem surprising since no difference was observed in the long range part of the mixing for a- and c-Si. Apparently, the short range order associated with covalent bonding plays a role in the mixing beyond $\sim$ 5 Å. The influence of short-range order can be understood by noting that, e.g., the cross section for Si recoils with energy less than 400 eV to scatter by more than 30° in subsequent collisions is 2 Å^2. Since this is comparable to the atomic size of Si atoms and to unfilled spaces in the open tetrahedral structure of a- and c-Si, there is some transparency to low energy recoils. In the close packed fcc structure, the dimensions of open spaces are much smaller so the transparency is reduced. These findings illustrate that once the collisional cross section increases to the size of the atomic radii, the crystal structure of the target influences the atom trajectories, even in nonchanneling directions.

We tested this idea concerning crystal structure by calculating ranges of low-energy self-atoms recoiling from an ideal lattice position in Si and Al with the MDRANGE method.[11] The recoil was initially placed on an ideal lattice site (or the site of an existing atom in a-Si), and given a recoil velocities randomly selected to cover all crystal directions. To obtain a representative picture of ranges from non-

TABLE II. Range results for low-energy self-ions in crystalline Si and Al at a temperature of 77 K. The results for each case are averages over 2000 events. The uncertainty of the straggling (second moment of the range distribution) results is half of the range uncertainty. Range results in the artificial fcc Si structure are included to illustrate the effect of the crystal structure on the range results.

Element	E (eV)	$\bar{R}$ (Å)	Straggle (Å)	$\langle R_{rec}^2 \rangle$
c-Si	100	9.0±0.1	2.6	88
	200	13.0±0.2	4.9	200
	400	21.0±0.3	10.0	530
a-Si[a]	100	9.6±0.1	3.4	105
	200	14.3±0.2	5.6	195
	400	21.3±0.2	8.7	530
c-Al	100	6.8±0.1	1.8	49
	200	9.2±0.1	2.7	90
	400	14.5±0.1	5.4	240
a-Al[b]	100	8.3±0.1	2.7	76
	200	12.8±0.2	4.8	190
	400	20.1±0.3	8.2	470
fcc Si (a=4.31)	100	7.8±0.1	2.2	65
	200	11.4±0.2	3.9	145
	400	18.9±0.2	9.0	450
c-Ge	100	6.1±0.1	1.2	39
	200	9.8±0.2	3.2	107
	400	13.3±0.2	5.3	207
a-Ge[b]	100	6.1±0.1	1.9	41
	200	9.0±0.2	3.3	92
	400	13.3±0.2	5.1	212
c-Cu	100	3.0±0.1	0.5	9
	200	4.1±0.1	0.8	18
	400	6.0±0.1	1.5	38

[a]*Ab initio* amorphous Si structure from Ref. 26.
[b]Amorphous structure obtained from MD simulations in the present work.

FIG. 5. As Fig. 1, but for Al.

equivalent lattice sites in amorphous materials, the range results were calculated as the average over recoils starting from several initial sites. The chord (vector) range[25] was used to quantify the displacement of the initial ion.

The range results show that both the range and straggling are larger for Si than for Al (see Table II). The larger number of long-range recoils produces a significant increase in the mean square atom displacement of the recoiling atom $\langle R_{rec}^2 \rangle$ relevant for mixing. The results for a-Si are quite close to those of c-Si. To verify that the Si–Al difference is not simply a consequence of the 20% lower atomic density of Si, we calculated Si ranges in an fcc structure at the normal silicon density. The obtained $\langle R_{rec}^2 \rangle$ results are roughly in the middle between c-Si and c-Al, confirming that the density change alone does not account for the increased mixing in c-Si compared to c-Al.

Table I shows that the mixing in amorphous aluminum is substantially larger than that in c-Al. Figure 5 illustrates the dependence of the mixing on the atom displacement distance. The short range contribution to the mixing is dramatically larger in a- than in c-Al; about 80% of the mixing in the amorphous material derives from mixing at atomic displacements shorter than 5 Å. There are two reasons to this phenomenon. First, as in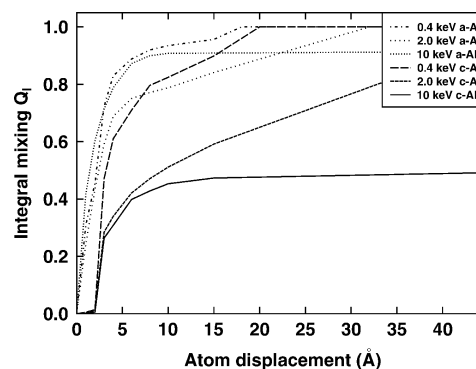 silicon, the atoms in the amorphous material can rearrange to new random sites at the end of the cascade, whereas in c-Al they are forced back to a lattice site, which in many cases is their nascent lattice site. Since no residual amorphous zones form in the cascade region of c-Al, the difference in mixing between c- and a-Al is more pronounced than the difference between c- and a-Si. Second, the amorphous material conducts heat more slowly than the crystalline one, making the liquid larger and its cooling time longer (e.g., for the 2 keV cases, the liquid in a-Al is on average about 1.5 times bigger and cools two times slower than in c-Al). Since the fcc metals form denser cascades than the tetrahedral semiconductors, this adds to the short- and medium-range mixing much more than in Si.

The long-range mixing $Q - Q'$ is also larger in a-Al than in c-Al. This is explained by the range results in Table II, which show that $\langle R_{rec}^2 \rangle$ for medium-energy secondary recoils in a-Al is about twice that in c-Al. Even though our amorphous aluminum structure retains considerable short-range order, the shielding of an atom starting from a lattice site is not as effective as in the perfect structure, making it easier for atoms in a-Al to find open directions. Notice too that the long range mixing in a-Al is only slightly smaller than that in a-Si. The increase in the total mixing due to these longer range recoils, however, is small compared to the increase caused by the small atom displacements described above.

B. Heavy materials

The mixing results for 10 keV self-recoils in c-Ge, a-Ge, c-Ni, c-Cu, c-Pt, c-Au, and a-Au are shown in Table I. Comparison of the results in crystalline Ge and Cu show that mixing in the tetrahedral semiconductor Ge is approximately twice that in the fcc metal Cu, even though Ge and Cu have comparable masses and melting points. This result is understood to a large extent by the contribution of longer-range recoils to the mixing, similar to that observed in the comparison between Si and Al. The range results for 100–400 eV recoils in Ge and Cu in Table III show a very large difference in the ranges of medium-energy recoils. Because the atomic density of Ge is about half that of Cu, this relative difference in Ge and Cu is more pronounced than in Si and Al. Thus, mixing in Ge is larger than in Cu due to the long-range mixing by ballistic recoils. Conversely, the mixing parameter is larger in Ge than Si due to the larger short-range
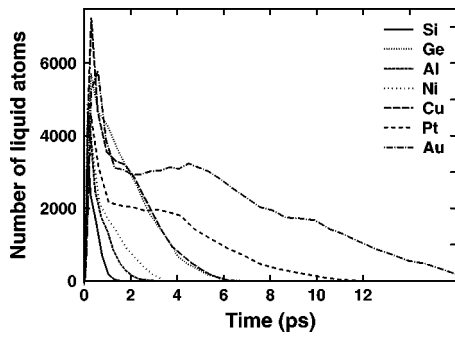
FIG. 6. Number of liquid atoms as a function of time in representative 10 keV cascades in the seven different elements.

FIG. 7. Mixing as a function of time for individual representative 10 keV cascade events in five fcc metals. The inset compares the mixing in c- and a-Au.

mixing in Ge. This part of the mixing is due to thermal spike effects as the melting point of Ge is 1200 K, while it is 1700 K in Si. While in c-Si we saw above that all the mixing is finished at 1–2 ps, in 10 keV cascades in crystalline Ge the mixing continues to increase until almost 10 ps due to relocation of atoms in the melt. We also observe that the mixing in a-Ge is about twice that in c-Ge and a factor of 6 larger than that in c-Cu. Analogously to the situation in a-Al and a-Si the enhanced mixing in the amorphous structure derived from short range mixing.

Comparison of the fcc metals Ni and Cu on one hand, and Pt and Au on the other hand, illustrates the importance of thermal spike effects in these materials. The mixing parameter is nearly three times higher in Cu and Au than in Ni and Pt, respectively. Since each metal of both pairs has nearly the same mass and atomic density, the ballistic part of the mixing is assured to be the same, leaving the thermal spike mixing to account for the differences. Within the present EAM model, the melting points of Ni, Cu, Pt, and Au are 1630, 1220, 1500, and 1100 K, respectively.[15] Also, the bulk modulus of Ni is about 1.4 times that of Cu, and that of Pt is 1.7 times that of Au. The lower melting points in Cu and Au cause the liquids in the center of the cascade to be roughly twice as large, and to exist twice as long, as those in Ni and Pt (Fig. 6). This increases both the number of atoms which can get redistributed in the liquid, and the distance they can move while in it. The elastic stiffness of the material appears to be also important for thermal spike diffusion since the atomic mobilities in cascades are very sensitive to the atomic densities. In materials with soft elastic properties, the pressures generated in the hot cascades greatly expand the lattice and enhance diffusion.

The time evolution of mixing in the five fcc metals is illustrated in Fig. 7 for 10 keV cascades. We see that the initial mixing in this series of metals, which is proportional to the size of the molten region formed in the heat spike, increases with decreasing melting temperature and elastic modulus. After the first few ps of the initial spike, the mixing reaches a maximum and then decreases as the pressure and heat waves outside the liquid region abate. This is partially due to atoms falling back on lattice sites, but also due to the increase in density in the center of the cascade as it cools. This latter effect can be understood by following the evolution of a typical 10 keV cascade in Au, for which this effect is largest.
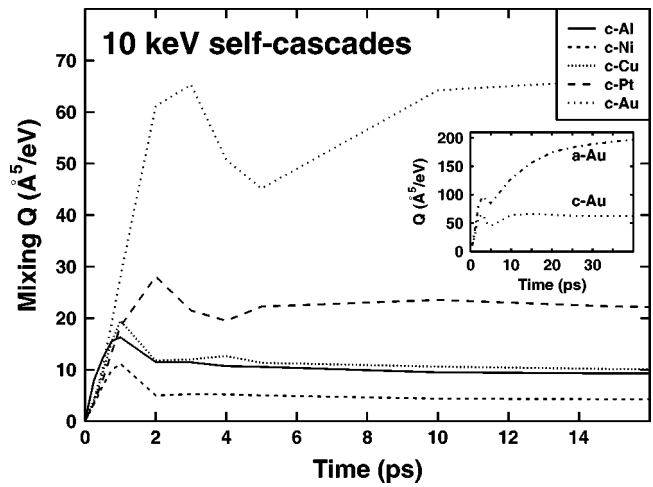
In Fig. 8 snapshots of atom positions in Au are shown at various instants in the cascade evolution. For clarity, only atoms within a cross-sectional slab of thickness $a_0/2$ through the center of the cascade are shown. During the first 3 ps, cavitation develops as the cascade expands outward. The extent of the expansion is largely controlled by the elastic modulus, which in Au is moderately low. The mixing is very large at this time due to the small atomic density in the central region. During the next 2 ps the cavity collapses, which coincides with the drop in the mixing parameter. The reduction in the mixing parameter during this time derives from the movement of atoms back to the center of the cascade. In Au, mixing in the melt continues after the cavitation has collapsed, although most of the mixing occurs in the earlier phase of the cascade. The final relocated atoms (shown as hollow spheres at 30 ps in Fig. 8) are located in the same cell region which was molten during the first 1–3 ps of the cascade. Notice that nearly every atom in the liquid core has relocated. Figure 9 illustrates the fractional mixing Q_r as a function of the relocation distance of different metals. All materials have a peak in the mixing at the nearest-neighbor distance. While the mixing in Ni predominantly derives from this short-range mixing, in Cu, Au, and Pt, where the molten region exists for a long time (cf. Fig. 6), a large fraction of the mixing derives from atoms relocated 5–20 Å from their initial site during the cascade evolution.

The mixing in a-Au is much larger than in its crystalline counterpart. The inset in Fig. 7 shows that although the initial a-Au mixing is not much different from that in c-Au, the mixing continues to increase for about 40 ps after the cascade. Inspection of the events showed that the liquid exists for about 25 ps after the cascade was initiated, so the increase in mixing is a consequence of both the mixing in the liquid zone, and the local rearrangements of atoms in the amorphous material. In the four materials investigated, Si, Al, Ge, and Au, mixing in the amorphous phase is 2–3 times larger than in the crystalline phase. This result is rather remarkable since the difference in the cohesive energy between the crystalline and amorphous phase is rather negligible, in-
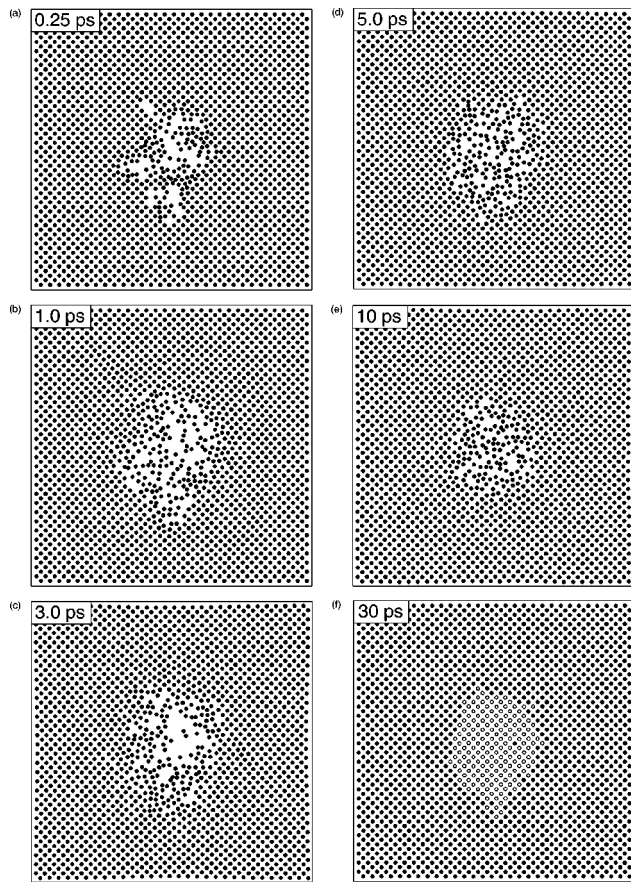
FIG. 8. Cross sections of the evolution of a 10 keV cascade in Au. The sections show a slice with a size of $30 \times 30 \times \frac{1}{2} a_0$ in the center of the cell. During the first 3 ps a large, almost void atom region is formed in the center of the cell, but it collapses back and (in this particular z slice shown) regenerates into perfect crystal. In the final 30 ps figure the atoms that are not at their original positions are indicated with hollow circles.

dicating that the cohesive energy is not the critical parameter controlling mixing as has been suggested in the literature.[27]

C. Comparison with experiment

Our finding that secondary recoils contribute significantly to atom relocation in semiconductors is in excellent qualitative agreement with the experimental evidence by Keinonen *et al.* of a large mixing contribution from low-
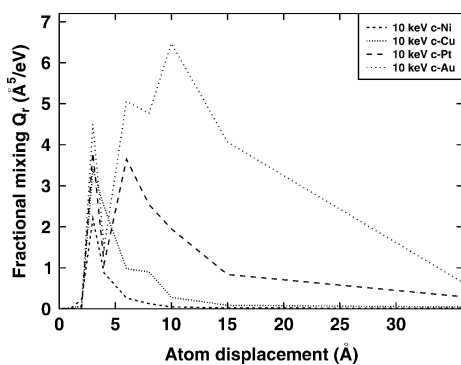

FIG. 9. Fractional mixing Q_r, i.e., mixing as a function of the atom displacement distance for 10 keV cascades in the five fcc metals.

TABLE III. Simulated (sim.) and measured (exp.) values for the mixing coefficient Q. All values are in units of $Å^5$/eV. For Si and Ge, the average (ave.) mixing over all marker elements is given along with that for a Ge or Si marker.

Material	Q (sim.)	Q (exp.)	Marker element
c-Si	15	80, 60	Ge, ave.[a]
a-Si	30	80, 60	Ge, ave.[a]
c-Ge	30	90, 120	Si, ave.[a]
a-Ge	70	90, 120	Si, ave.[a]
Al	9	13–23	Ag, W, Pt[b]
Ni	4	5–8	Pt, Au[b]
Cu	14	23–27	Cu Ref. 1; Pt, Au[b]
Pt	22	14, 24	Fe, Ni[b]
Au	58	60, 160	Ni, Cu[b]

[a]Reference 1.
[b]Reference 28.

energy recoils in Si.[5] Our results show that this effect is a consequence of the open crystal structure in Si and should not be expected to be pronounced in materials with close-packed structures.

The experimentally measured mixing efficiency is usually defined as

$$Q_{\mathrm{exp}} = \frac{Dt}{\Phi F_{D_n}}, \qquad (3)$$

where D is an effective diffusion coefficient for mixing, t is the implantation time, Φ the ion fluence, and F_{D_n} the deposited nuclear energy per ion per unit depth.[28] The equivalence between Q_{exp} and the simulated mixing Q given in Eq. (1) follows from the atomistic definition of the diffusion coefficient.[29,30] Despite the equivalence between these definitions of mixing, the quantitative comparison of our results with experiments is not completely direct. Most irradiations have been performed using ions with masses ranging from 20 amu (Ne) to 136 amu (Xe) and with ion energies much higher than the ones used here, typically over 100 keV.[1] The comparison is further complicated by procedures employed to obtain the mixing parameter. The experimental values are usually obtained by fitting a Gaussian profile to the broadened marker layer shape. Since the distribution of recoiled atom with displacement distance actually falls off in materials such as Si as $1/r^2$ (Fig. 2), the shape of the broadened marker layer will not necessarily have an ideally Gaussian shape.[31] Thus, the mixing derived from fits to Gaussian distribution may not correspond exactly to the atomic mixing obtained from simulations. Despite these complications, useful comparisons are possible, largely because energetic cascades break up into subcascade structure, and the energy dependence of the mixing parameter is relatively weak.[32] Subcascade formation begins below or not far above ~10 keV for all but the Au and Pt events.

The mixing parameters obtained from our simulations are compared with experiments in Table III. The experimental results are obtained from various sources. For the metals, we chose the experimental values from the measurements of Kim *et al.*,[28] since they were performed at 6 K using markers with similar characteristics as the host metals themselves, and thus most suitable for our self-ion simulations at 0 K. For Si and Ge we used results from the review by Paine and

Averback.[1] Values for Si markers in Ge and Ge markers in Si are listed, as these seem most appropriate, and the average mixing value of all the markers is given for each host. Because the values of mixing vary by a factor of ~ 2 from marker to another, agreement between simulations and experiments can only be considered at this level.

The overall agreement between simulation and experiment is relatively good, even on an absolute scale. In all cases the values obtained by simulation are within a factor of 2 of those obtained by experiment. Except for the case of Pt, the simulation values are smaller than the experimental ones. This can be explained by the possibility that the mixing parameters have not yet reached their asymptotic ''subcascade'' values at 10 keV. Diaz de la Rubia *et al.* found for Cu that the mixing parameter increased by a factor of 60% between 10 and 25 keV.[33] For Au and Pt, subcascade formation is not expected until about 50 keV.[34]

The simulations are particularly successful in predicting the relative values of the mixing parameters. In comparing mixing in *a*-Si and *a*-Ge with that in Al and Cu, both the simulation and experiments show a factor of about 3 times larger mixing in the amorphous semiconductors. This was explained above on the basis of the open, amorphous structure in these materials. The difference in experimental mixing values by a factor of ~ 3 between Cu and Ni on one hand, and Pt and Au on the other hand, is also reproduced in the simulations. Since electron–phonon coupling has not been included in the simulation, the results appear to be in contradiction with the model of Koponen,[4] which suggests that the electron–phonon coupling can explain the low mixing of Ni and Pt compared to that in Cu and Au (although a later article mentions that this is not the only possible explanation for the difference.)[35]

Our results, moreover, are readily compared with those in Koponen's article since the average deposited energies of about 200 eV/Å for Ni and Cu, and 300 eV/Å for Au and Pt used there are about the same as in our simulations (the mean range of 10 keV Ni and Cu self-recoils is about 45 Å, and 10 keV Au and Pt recoils is 30 Å).[15] Although the question of electron–phonon coupling will be further discussed below, it can be seen that much of the difference in the mixing between Cu and Ni, and between Au and Pt, can be attributed to their different melting temperatures and elastic properties. Our mixing values of 4 and 22 for Ni and Pt are in clearly better agreement with experiment than the very low values of 1–2 and 5 given by the model of Koponen.[4]

Before discounting the possible importance of electron–phonon coupling, it is worth noting that only for Pt the simulated values of the mixing parameter are as large, or larger, than the experimental ones. This is surprising since 10 keV recoils are far below the subcascade regime in Pt so that even higher mixing values can be expected at higher energies. In the other materials, it is unlikely that higher energies would raise the simulated mixing values above the experimental ones. For this reason, we ran three additional cascades of 25 keV in Pt. A mixing parameter of 45 Å^5/eV was obtained. This value is clearly higher than the experimental ones, and if we assume that subcascade formation does not become prominent until 50 keV, even higher values of the mixing parameter may be found for the actual experimental recoil energies.

These findings suggest, therefore, that the simulated values of mixing in Pt are too high, albeit only by a factor of 2 or less. This may be related to the Pt potential underestimating the experimental melting point by about 500 K, more than any of the other potentials.[36] Another possible explanation appears to be the exclusion of electron–phonon coupling from the calculations, although deficiencies in the interatomic potential for Pt cannot be completely ruled out. If electron–phonon coupling is indeed responsible for the discrepancy between simulation and experiment, these findings will have significance for mixing in many other metals as well, as discussed by Flynn and Averback.[37] Nevertheless, since the calculated mixing in Au is a factor of ~ 3 greater than that in Pt (at 10 keV), it is clear that the crystal structure, melting temperature, and elastic properties of the material are still dominant factors in understanding ion beam mixing in most materials. Since the mixing is a direct consequence of the general time development of a collision cascade, it is likely that this conclusion holds for many other aspects of cascade evolution as well.

IV. CONCLUSIONS

The present work has examined the mechanisms of mixing in several crystalline and amorphous semiconductors and metals. A primary observation was that mixing in the amorphous phase is larger by a factor of $\sim 2-3$ than in the crystalline counterpart. In Si the enhanced mixing is primarily due to relaxation effects following the ballistic phase of the cascade, while in metals it is due to the extended lifetime of the thermal spike. A new finding in this study concerned the role of the local structural order on the range of low energy particles is revealed. It was found that the more open structures associated with tetrahedral bonding provide some transparency for low energy particles, allowing them to traverse much farther than they can in close-packed structures. It was shown that this is not simply a question of atomic density. The larger mixing in semiconductors than in corresponding metals appears to be a consequence of their more open structures and their amorphous structures under irradiation.

In metals, we obtained fairly good agreement with experiment even though we did not include the electron–phonon coupling in the simulations. In all cases, the simulated values of the mixing parameter were within a factor of 2 of the experimental values, and even this discrepancy could be attributed to the different recoil spectra employed in the simulation and experiments. The ratios in mixing between Ni and Cu and Pt and Au showed that basic material characteristics like the melting temperature can account for a large difference in mixing in materials with similar densities and masses, which indicates that the electron–phonon coupling may not be as important in cascades in Pt and Ni as previously thought. Additional mixing experiments in Ni and Pt using irradiations with lower energy recoil spectra would greatly help in establishing the role of electron–phonon coupling in this material.

[1] See, for example, B. M. Paine and R. S. Averback, Nucl. Instrum. Methods Phys. Res. B **7/8**, 666 (1985).

[2] D. V. Forbes, J. J. Coleman, J. L. Klatt, and R. S. Averback, J. Appl. Phys. **77**, 3543 (1995).

[3] W. Bolse, Mater. Sci. Eng. R. Rep. **12**, 53 (1994).

[4] I. Koponen, J. Appl. Phys. **72**, 1194 (1992).

[5] J. Keinonen, M. Hautala, I. Koponen, and M. Erola, Phys. Rev. B **41**, 9907 (1990).

[6] J. L. Klatt, R. S. Averback, and D. Peak, Appl. Phys. Lett. **55**, 1295 (1989).

[7] P. Sigmund and A. Gras-Marti, Nucl. Instrum. Method Phys. Res. B **182/183**, 25 (1981).

[8] M. J. Caturla, V. Konoplev, I. Abril, and A. Gras-Marti, Nucl. Instrum. Methods Phys. Res. B **102**, 19 (1995).

[9] K. Nordlund and R. S. Averback, Appl. Phys. Lett. **70**, 3103 (1997).

[10] M. P. Allen and D. J. Tildesley, *Computer Simulation of Liquids* (Oxford University Press, Oxford, England, 1989).

[11] K. Nordlund, Comput. Mater. Sci. **3**, 448 (1995).

[12] H. J. C. Berendsen, J. P. M. Postma, W. F. van Gunsteren, A. DiNola, and J. R. Haak, J. Chem. Phys. **81**, 3684 (1984).

[13] F. H. Stillinger and T. A. Weber, Phys. Rev. B **31**, 5262 (1985).

[14] H. Balamane, T. Halicioglu, and W. A. Tiller, Phys. Rev. B **46**, 2250 (1992).

[15] K. Nordlund, M. Ghaly, R. S. Averback, M. Caturla, T. Diaz de la Rubia, and J. Tarus, Phys. Rev. B (submitted).

[16] K. Nordlund, N. Runeberg, and D. Sundholm, Nucl. Instrum. Method. Phys. Res. B (in press).

[17] K. Nordlund, J. Keinonen, and T. Mattila, Phys. Rev. Lett. **77**, 699 (1996).

[18] F. Ercolessi and J. B. Adams, Europhys. Lett. **26**, 583 (1994).

[19] M. S. Daw, S. M. Foiles, and M. I. Baskes, Mater. Sci. Rep. **9**, 251 (1993).

[20] J. F. Ziegler J. P. Biersack, and U. Littmark, *The Stopping and Range of Ions in Matter* (Pergamon, New York, 1985).

[21] A. V. Granato, Phys. Rev. Lett. **68**, 974 (1992).

[22] J. Keinonen, K. Arstila, and P. Tikkanen, Appl. Phys. Lett. **60**, 228 (1992).

[23] J. F. Ziegler, SRIM-96 computer code, private communication.

[24] Because of the large volume of the liquid in gold, the 10 Å cutoff is not very meaningful in this material. Therefore, the short-range mixing in gold is not discussed in the text.

[25] J. Lindhard, M. Scharff, and H. E. Shiøtt, Mat. Fys. Medd. K. Dan. Vidensk. Selsk. **33**, 1 (1963).

[26] P. A. Fedders, D. A. Drabold, and S. Klemm, Phys. Rev. B **45**, 4048 (1992).

[27] W. L. Johnson, Y. T. Cheng, M. van Rossum, and M.-A. Nicolet, Nucl. Instrum. Method Phys. Res. B **7/8**, 657 (1985).

[28] S.-J. Kim, M.-A. Nicolet, R. S. Averback, and D. Peak, Phys. Rev. B **37**, 38 (1988).

[29] T. Diaz de la Rubia and R. S. Averback, Phys. Rev. Lett. **59**, 1930 (1987).

[30] N. L. Peterson, J. Nucl. Mater. **69&70**, 3 (1978).

[31] We checked this by a Monte Carlo simulation of the broadening of marker layer atoms with $1/r^2$ displacements. The resulting profiles did not have a Gaussian shape even after a very large number of successive displacement steps.

[32] D. J. Bacon and T. Diaz de la Rubia, J. Nucl. Mater. **216**, 275 (1994).

[33] T. Diaz de la Rubia and M. W. Guinan, Mater. Res. Forum **97–99**, 23 (1992).

[34] K. L. Merkle, in *Radiation Damage in Metals*, edited by N. L. Peterson and S. D. Harkness (American Society for Metals, Metals Park, OH, 1976), p. 58.

[35] I. Koponen, Phys. Rev. B **47**, 14011 (1993).

[36] Test simulations with a Pt EAM potential with a corrected melting point indicates the melting point difference may have a significant effect on the mixing results in Pt. Results of these calculations will be published later.

[37] C. P. Flynn and R. S. Averback, Phys. Rev. B **38**, 7118 (1988).